Palaeogeography, Palaeoclimatology, Palaeoecology 655 (2024) 112562

Contents lists available at ScienceDirect

Palaeogeography, Palaeoclimatology, Palaeoecology

journal homepage: www.elsevier.com/locate/palaeo

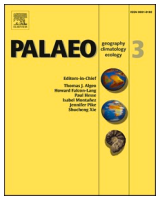

Editorial preface to special issue: Response of marine and terrestrial environments to Triassic–Paleogene hyperthermals

Zhong Han [a,*], Santanu Banerjee [b], Jacopo Dal Corso [c], Xiumian Hu [d], David B. Kemp [e]

[a] Key Laboratory of Oil and Gas Reservoir Geology and Exploitation and Key Laboratory of Deep-time Geography and Environment Reconstruction and Applications, MNR, Institute of Sedimentary Geology, Chengdu University of Technology, Chengdu 610059, China
[b] Department of Earth Sciences, Indian Institute of Technology Bombay, Powai, Mumbai 400076, India
[c] State Key Laboratory of Biogeology and Environmental Geology, China University of Geosciences, Wuhan 430074, China
[d] State Key Laboratory of Mineral Deposit Research, School of Earth Sciences and Engineering, Nanjing University, Nanjing 210023, China
[e] State Key Laboratory of Biogeology and Environmental Geology and Hubei Key Laboratory for Critical Zone Evolution, School of Earth Sciences, China University of Geosciences, Wuhan 430074, China

ARTICLE INFO

Editor: Dr. Howard Falcon-Lang

Keywords:
Mesozoic–Paleogene
Hyperthermal events
Carbon cycle perturbations
Climate and environmental change

ABSTRACT

The Mesozoic–Paleogene hyperthermals represent critical intervals of rapid global warming associated with abrupt carbon cycle perturbations. These events can provide valuable deep-time insights into how climate might respond to the current rise in temperatures driven by anthropogenic greenhouse gas emissions. This special issue comprises 17 publications that cover a broad spectrum of the research on hyperthermals, and these can be grouped into four main themes: (1) carbon-cycle perturbations, (2) environmental changes and biogeochemical extremes, (3) biotic responses to warming, and (4) long-term climatic and environmental changes in greenhouse climates. By integrating sedimentological, geochemical, and paleontological methods, the studies in this issue explore carbon sources and release mechanisms, provide insights into the initiation, development, and termination of hyperthermal events, and elucidate their longer-term impacts. The studies provide new insights into the interactions between short-term extreme events and long-term climate trends, offering valuable perspectives on the future trajectory of Earth's climate in response to ongoing anthropogenic warming.

1. Introduction

The alternating climate states of hothouse, warmhouse, coolhouse, and icehouse have played a significant role in shaping Earth's history (Scotese et al., 2021; Judd et al., 2024). The Mesozoic–Paleogene (from the Permian–Triassic boundary to the middle Eocene, ~252 to 40 Ma) was a pivotal period in Earth's evolution toward its modern state, which witnessed the breakup of the supercontinent Pangaea, widespread large igneous province (LIP) volcanism, and significant biotic crisis and innovations (Ernst and Youbi, 2017; Percival et al., 2018; Gernon et al., 2024). Importantly, a series of short-lived hyperthermal events punctuated this interval of Earth history. Notable hyperthermal events include the Permian–Triassic Boundary Event, Carnian Pluvial Episode, Triassic–Jurassic Boundary Event, the Early Jurassic and Cretaceous Oceanic Anoxic Events, Paleocene–Eocene Thermal Maximum, and Middle Eocene Climatic Optimum (Fig. 1). These events were commonly associated with massive, rapid release of isotopically light carbon into ocean−atmosphere system, resulting in large-scale global warming. They shared similar changes in paleoecology, paleoenvironment and paleoclimate, i.e. elevated rates of marine and terrestrial extinction, increased atmospheric CO_2 levels, intensified hydrological cycling, elevated continental weathering, and changes in ocean chemistry (e.g., Foster et al., 2018; Hu et al., 2020; Westerhold et al., 2020). Consequently, these transient hyperthermal events provide crucial insights into the mechanisms that drive climate change, and have potential parallels to rapid modern anthropogenic warming (Tierney et al., 2020; Mancini et al., 2024). Additionally, long-term climate changes create the conditions under which short-term extreme events are more likely to occur, while the frequent occurrence of such events may, in turn, accelerate the progression of longer-term climate change. Understanding these interactions is a crucial focus of paleoclimate research.

The contributions of this virtual special issue (VSI) focus on the

* Corresponding author.
E-mail addresses: hanzhong19@cdut.edu.cn (Z. Han), santanu@iitb.ac.in (S. Banerjee), j.dalcorso@cug.edu.cn (J.D. Corso), huxm@nju.edu.cn (X. Hu), davidkemp@cug.edu.cn (D.B. Kemp).

https://doi.org/10.1016/j.palaeo.2024.112562
Received 13 October 2024; Accepted 14 October 2024
Available online 16 October 2024

major hyperthermals of the Triassic–Paleogene (Table 1), forming a collection that sheds light on the marine and terrestrial environmental changes and biological responses to these events (Fig. 2). The transient hyperthermals include End-Permian–Triassic Mass Extinction Event, Toarcian Oceanic Anoxic Event/or Jenkyns Event, Oceanic Anoxic Event 1d and 2, Paleocene–Eocene Thermal Maximum and Middle Eocene Climatic Optimum, while the longer-term events include intervals of the Middle Jurassic, Middle and Late Cretaceous, Cretaceous–Paleogene transition, Early Eocene (Table 1). The methods of sedimentology, geochemistry, paleontology, data statistics, and paleoclimate Earth system modeling were used to explored the carbon isotope perturbations, redox conditions, continental hydrology, temperature changes and biogeochemical responses associated with these pivotal episodes, offering a deeper understanding of the environmental drivers and consequences of past climate crises.

2. Carbon-cycle perturbations

Ancient hyperthermal events of the Mesozoic–Paleogene are typically linked to brief negative and/or positive carbon isotope excursions recorded in both marine and terrestrial sediments (e.g., Permian–-Triassic Boundary Event, Carnian Pluvial Episode, Triassic–Jurassic Boundary Event, Early Jurassic and Cretaceous Oceanic Anoxic Events and Paleocene–Eocene Thermal Maximum) (Jenkyns, 2010; Clapham and Renne, 2019; Hu et al., 2020; Gradstein et al., 2020). These carbon-isotope excursions demonstrate that these events were generally affected by transient carbon-cycle perturbations, which in turn modulated the Earth's climatic, environmental and biological system. These carbon-isotope perturbations are crucial for investigating carbon sources and release mechanisms into the atmosphere–ocean system, as well as carbon emission rates. Moreover, carbon isotope data serve as an effective tool for global correlation.

High-resolution carbon-isotope data from carbonate platforms can highlight the significant impacts of carbon cycle disruption on shallow water ecosystems. He et al. (2024, this VSI; Fig. 1.2a-c) investigated the sedimentary evolution of carbonate platforms across the hyperthermal event at Permian–Triassic boundary (PTB), which was the largest mass extinction in Earth history. By analyzing three carbonate platform sections from South China and the Lhasa Terrane, they demonstrated significant environmental changes during this event. Their data reveal a clear correspondence between shifts in carbonate production and the negative carbon-isotope excursion (NCIE), which can be divided into four stages (NC1 to NC4). The onset of the NCIE is marked by a transition in carbonate facies, with a carbonate production crisis observed 11 kyr after the NCIE's onset, preceding the first mass extinction event. The results suggest that volcanic CO_2 emissions from the Siberian Traps LIP likely contributed to the environmental stresses that led to both the carbonate production crisis and the mass extinctions. In addition, the development of anachronistic facies, including microbialites and dolomites, is linked to widespread deoxygenation and ocean acidification during the PTB.

Wang et al. (2024a, this VSI; Fig. 1.2d) present a carbon-isotope analysis of pedogenic carbonates from matured calcisols in the Nanxiong Basin, South China, to detect terrestrial carbon cycle changes and reconstruct atmospheric CO_2 concentrations (pCO_2) from ~76.0 to 62.0 Ma, i.e., across the Cretaceous–Paleogene (K-Pg) mass extinction. Carbon cycle variations are shown by marked $\delta^{13}C$ changes through the K-Pg, indicating a process of deterioration, stabilization and recovery of terrestrial ecosystems in the aftermath of the mass extinction. The fluctuations observed in the estimated pCO_2 levels align with sea surface temperature records, attesting to a strong perturbation of climate coeval with the carbon cycle variations. In addition, the study elucidates long-

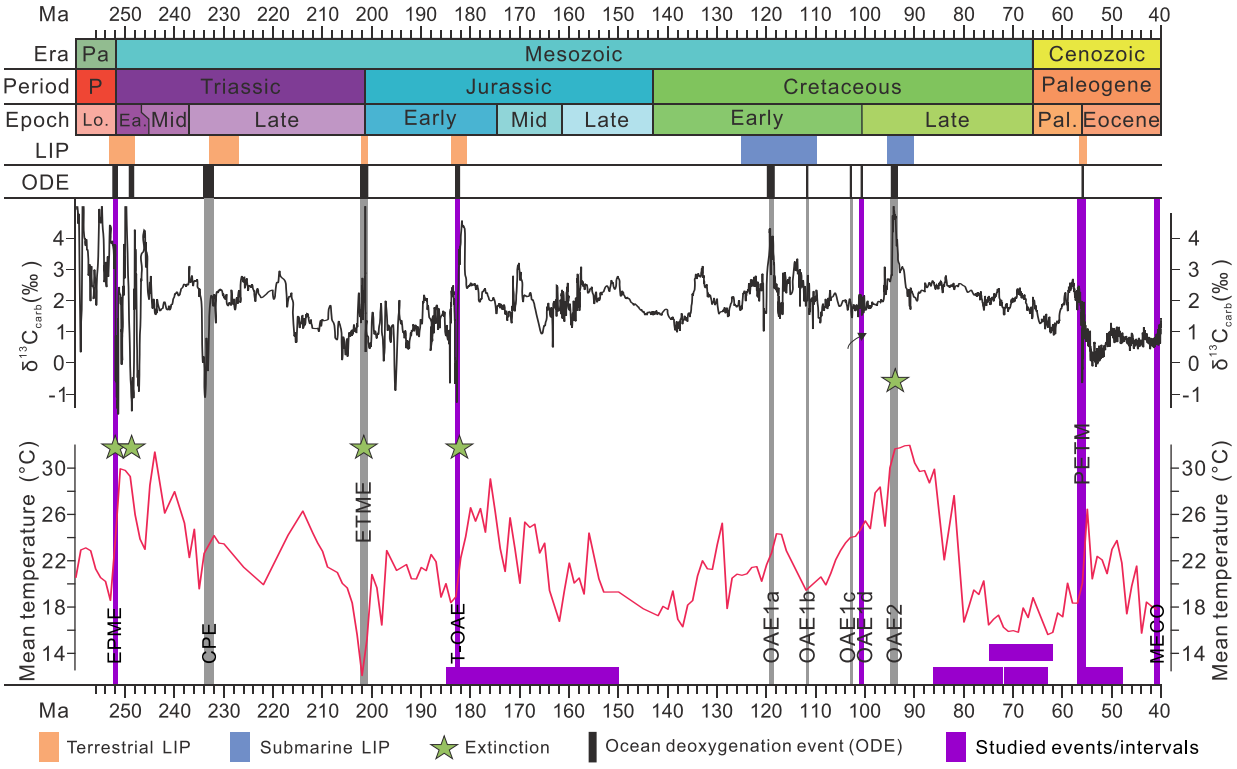

Fig. 1. Integrated data on temperature changes, carbon cycle disturbances, and large igneous province (LIP) events during the Mesozoic–Paleogene, modified from the compiled figure of He et al. (2023). Key events are shown on the geological time scale (Gradstein et al., 2020), including the Permian–Triassic Mass Extinction (PTME), End–Triassic Mass Extinction (ETME), Carnian Pluvial Episode (CPE), Toarcian Oceanic Anoxic Event (TOAE), Cretaceous Oceanic Anoxic Events (OAE 1a, 1b, 1c, 1d, and 2), Paleocene–Eocene Thermal Maximum (PETM), and Middle Eocene Climatic Optimum (MECP). The events and time periods studied in the papers in this special issue are highlighted in purple. (For interpretation of the references to colour in this figure legend, the reader is referred to the web version of this article.)

Table 1
Summary of studied sites, sedimentary environment, key events, age/period, and topics in this special issue.

No	Title	Study sites	Environment	Events/Interval	Age/Period (Ma)	Topic	References
1	High terrestrial temperature in the low-latitude Nanxiong Basin during the Cretaceous-Paleogene boundary interval	Nanxiong Basin, South China	Lacustrine	Cretaceous-Paleogene boundary	~71.9–62.8	Rapid warming and LIP	Yin et al., 2023
2	The sedimentological characteristics of the intermontane desert system in the Jurong Basin, South China and its relationship with the Late Cretaceous hot climate	Jurong Basin, South China	Fluvial and lacustrine	Late Cretaceous	~86.3–72.1	Hot climate controls on desert development	Cao et al., 2023
3	Carbonate factories and their critical control on the geometry of carbonate platforms (mid-Cretaceous, southern Iran)	Zagros basin, southern Iran	Shallow marine	Middle Cretaceous	~120–94	Sea level controls and carbonate platform geometry	Xu et al., 2024
4	Benthic biota (nummulites) response to a hyperthermal event: Eccentricity-modulated precession control on climate during the middle Eocene warming in the Southern Mediterranean	Southern Mediterranean, Tunisia	Shallow marine	Middle Eocene (MECO)	~40.6–40.0	Foraminifer response and cyclostratigraphy	Messaoud et al., 2023
5	Biogeochemical responses to global warming during the Paleocene-Eocene Thermal Maximum in eastern Tethys	Tarim basin, northwest China	Shallow marine	Paleocene–Eocene Thermal Maximum (PETM)	~56	Biogeochemical responses	Wu et al., 2024
6	Mercury sequestration pathways under varying depositional conditions during Early Jurassic (Pliensbachian and Toarcian) Karoo-Ferrar volcanism	Cardigan Bay Basin, Wales, UK and Subbetic Basin, SE Spain	Epicontinental shelf	Toarcian Oceanic Anoxic Event (T-OAE)	~183	Mercury sequestration and volcanism	Kovács et al., 2024
7	Clumped isotope records of terrestrial temperatures during the Middle Jurassic (180–150 Ma) in East China	Sichuan, Zigui and Jiyuan Basin, China	Lacustrine	Middle Jurassic	~185–150	Terrestrial temperature	Jin et al., 2024
8	Ichnological response to the Middle Eocene Climatic Optimum (MECO) in the Bartonian deposits of Kutch Basin, India	Kutch Basin, western India	Shallow marine	Middle Eocene (MECO)	~40.6–40.0	Ichnological response	Das et al., 2024a
9	Impact of early Eocene (Ypresian) warming events on ichnological assemblage of the Naredi Formation, western Kutch (Kachchh) Basin of Gujarat, India	Kutch Basin, western India	Shallow marine	Early Eocene	~56–47.8	Ichnological response	Das et al., 2024b
10	Strontium isotope evidence for regional enhanced continental weathering during the early Toarcian in the Tethys Himalaya	Tibetan Himalaya, China	Shallow marine	Toarcian Oceanic Anoxic Event (T-OAE)	~183	Continental weatheirng	Yang et al., 2024
11	Polycyclic aromatic hydrocarbons (PAHs) evidence for frequent combustion events on land during the Permian–Triassic transition in Northwest China	Junggar Basin, Xinjiang	Fluvial-lacustrine	End-Permian mass extinction (EPME)	~252	Combustion events on land	Jiao et al., 2024
12	Long-term variations in terrestrial carbon cycles and atmospheric CO2 levels: Exploring impacts on global ecosystem and climate in the aftermath of end-Cretaceous mass extinction	Nanxiong Basin, South China	Flooding plain and overbank	End-Cretaceous	~76–62	Carbon cycles and atmospheric CO2	Wang et al., 2024
13	Vegetation response to climate change during an Early Jurassic hyperthermal event (Jenkyns Event) from Northern China (Ordos Basin)	Erdos basin, North China	Lacustrine	Toarcian Oceanic Anoxic Event (T-OAE)	~183	Vegetation response	Baranyi et al., 2024
14	Lead-up and manifestation of the Oceanic Anoxic Event 2 at the DSDP Site 398 (Vigo Seamount, NW Iberian offshore): Palynological and geochemical insights	Vigo Seamount, NW Iberian offshore	Hemipelagic-pelagic marine	Oceanic Anoxic Event 2 (OAE 2)	~94	Palynological responses	Rodríguez-Barreiro et al., 2024
15	Paleoenvironment reconstruction of the eastern Tethys during the pre-onset excursion preceding the PETM	Tarim basin, northwest China	Shallow marine	Pre-onset excursion (POE) prior to the PETM	~56	Chemical weathering, ocean productivity, and redox condition	Dong et al., 2024
16	Millennial-scale sedimentary evolution of carbonate platforms during the Permian–Triassic boundary hyperthermal event	Lhasa terrane and south China	Shallow marine	Permian–Triassic boundary hyperthermal event	~252	Carbon cycles and sedimenrary responses	Yang et al., 2024
17	Elevated sea surface temperature and enhanced primary productivity during Ocean Anoxic Event 1d in the eastern Tethys: Calcareous nannofossil evidence from southern Tibet, China	Tibetan Himalaya, China	Shallow marine	Ocean Anoxic Event 1d (OAE 1d)	~120	Sea surface temperature and enhanced productivity	Wang et al., 2024

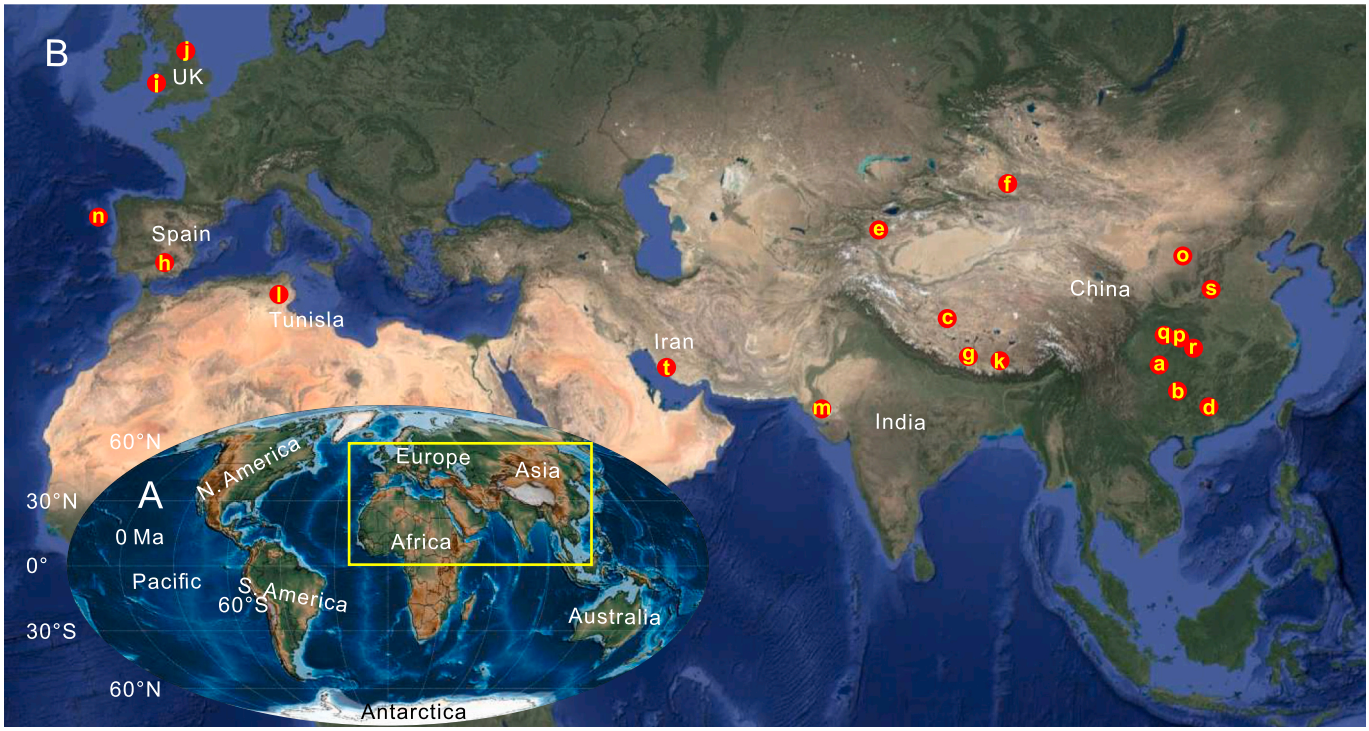

Fig. 2. Modern geographic map showing the study areas (A; 0 Ma, modified from Scotese (2021)) and enlarged geographic map (B; modified from Google map) showing study sections in our special issue. Letters refer to the following articles in this Special Issue (issue): a-Langfenya, b-Taiping and c-Wanbudangsang) He et al. (2024, this VSI); d-Datang) Wang et al. (2024a, this VSI); e-Kuzigongsu) Dong et al. (2024, this VSI); f-Dalongkou) Jiao et al. (2024, this VSI); g-Nianduo) Yang et al. (2024, this VSI); h-La Cerradura, i-Mochras borehole, j-Cleveland Basin) Kovács et al. (2024, this VSI); k-Chaqiela) Wang et al. (2024b, this VSI); e-Kuzigongsu) Wu et al. (2024, this VSI); l-Fejij) Jihede Haj Messaoud et al. (2023, this VSI); m-Kutch Basin) Das et al. (2024a, b, this VSI); n-389D) Rodríguez-Barreiro et al. (2024, this VSI); o- Anya) Baranyi et al. (2024, this VSI); p-Chishan) Cao et al. (2023, this VSI); q- Sichaun, r- Zigui, s- Jiyuan) Jin et al. (2024, this VSI); k-Datang) Yin et al. (2023, this VSI); t-Khormoj) Xu et al. (2023, this VSI).

term climate perturbations following Deccan Trap LIP eruption and the Chicxulub impact at the K-Pg boundary, of which the controlling factors remain to be fully understood.

Dong et al. (2024, this VSI; Fig. 1.2e) provide a comprehensive paleoenvironmental reconstruction of the Eastern Tethys during the so-called pre-onset excursion (POE), a warming event that preceded the Paleocene–Eocene Thermal Maximum (PETM). Unlike the more extensively studied PETM, the POE remains poorly understood, yet this research highlights its significant role in shaping subsequent climatic and environmental conditions. By analyzing high-resolution geochemical and magnetic susceptibility records from the well-preserved Kuzigongsu section in the Tarim Basin, the study provides evidence for intensified chemical weathering, increased primary productivity, and oceanic deoxygenation during the POE. Key proxies, such as the chemical index of alteration (CIA), Rb/Sr ratios and magnetic susceptibility, indicate that chemical weathering and river runoff were enhanced by elevated atmospheric CO_2. These conditions, in turn, contributed to higher marine productivity and a reduction in bottom water oxygen levels. This research underscores the POE's global significance as a precursor to the PETM and its potential as an analogue for understanding rapid climate changes driven by modern anthropogenic carbon emissions.

3. Environmental changes and biogeochemical extremes

The rapid release of isotopically light carbon into the ocean-atmosphere system and consequent global warming observed during Triassic−Paleogene hyperthermals resulted in profound environmental crises.

Jiao et al. (2024, this VSI; Fig. 1.2f) analyzed polycyclic aromatic hydrocarbons (PAHs) in sedimentary records from the Permian–Triassic (P–T) transition at the Dalongkou section in Northwest China. Their results indicate frequent high-temperature combustion events, driven by volcanic activity during this period. The study combines PAH ratios, mercury anomalies, and carbon-isotope data to suggest that wildfire events (in combination with volcanic eruptions) led to significant environmental disturbances. Increased PAH concentrations and shifts in their composition point to stepwise ecosystem collapse and soil erosion due to extreme climatic conditions – including aridification and increased wildfire frequency, across the P–T transition. These findings highlight the substantial impact of volcanic and wildfire events on terrestrial ecosystems during Earth's most severe extinction event.

Yang et al. (2024, this VSI; Fig. 1.2 g) investigated the early Toarcian Oceanic Anoxic Event (T-OAE) in the Tethys Himalaya by analyzing strontium isotopes ($^{87}Sr/^{86}Sr$) in carbonate rocks. Their findings show an abrupt positive shift in $^{87}Sr/^{86}Sr$ ratios beginning around the Pliensbachian–Toarcian boundary, which continued during the negative CIE that characterized the T-OAE. These data suggest enhanced continental weathering. The $^{87}Sr/^{86}Sr$ values gradually decrease during the recovery phase of the T-OAE CIE, indicating a decline in weathering intensity. The data also suggest that regional factors, such as increased terrigenous influx and diagenesis, likely influenced the strontium isotopic signal, though the global weathering response remains evident. Despite biases from diagenetic processes, the results highlight the importance of continental weathering in controlling seawater $^{87}Sr/^{86}Sr$ during the T-OAE in the eastern Tethys.

Kovács et al. (2024, this VSI; Fig. 1.2 h-j) examined mercury (Hg) sequestration pathways in three different Early Jurassic depositional environments during the T-OAE. This event coincided with Karoo/Ferrar LIP volcanism, and large amounts of Hg may have been emitted during this volcanism. Geochemical data and principal component analyses (PCA) reveal varied Hg associations with sedimentary parameters

across three basins: the anoxic-euxinic Cleveland Basin (Yorkshire, UK), the sub-oxic Cardigan Bay Basin (Wales, UK), and the oxygenated Subbetic Basin (SE Spain). In the Cleveland Basin, Hg is primarily associated with organic-sulphide-related elements, suggesting euxinic conditions played a major role in Hg sequestration. By contrast, Hg in the Cardigan Bay and Subbetic basins shows a closer association with redox-sensitive and detrital elements, highlighting the influence of depositional environment on Hg capture. The study emphasizes the spatial and temporal variability in Hg drawdown, influenced by local marine conditions and volcanic activity.

Wang et al. (2024b, this VSI; Fig. 1.2k) examined calcareous nannofossil assemblages from the middle-lower part of the Lengqingre Formation (Albian-Cenomanian) in the Chaqiela section, southern Tibet. Their refined nannofossil biostratigraphic analysis constrains the study interval to Upper Cretaceous (UC) Biozones UC0 through UC2, marking the Albian–Cenomanian boundary in the lower part of the Lengqingre Formation. This also dates the middle part to the Cenomanian and confirms the presence of the OAE 1d (around the Albian–Cenomanian boundary, ca. 100.5 Ma) in the section. Nutrient and temperature indices derived from nannofossil species data suggest elevated sea surface temperatures and enhanced productivity during OAE 1d in the southwestern shelf sea of the eastern Tethys Ocean.

Wu et al. (2024, this VSI; Fig. 1.2e) analyzed biogeochemical responses to the Paleocene–Eocene Thermal Maximum (PETM) in the eastern Tethys, focusing on the Tarim Basin in Northwest China. Their study reveals significant environmental shifts driven by rapid global warming and CO_2 emissions, likely linked to the emplacement of the North Atlantic Large Igneous Province. Chemical weathering proxies such as the chemical index of alteration (CIA) and clay mineral assemblages indicate intensified chemical and physical weathering, accompanied by increased terrestrial input. Additionally, nutrient-sensitive elements and an increase in calcareous nannofossils suggest heightened marine productivity during the PETM. The study also identifies episodic deoxygenation, as indicated by enrichments in redox-sensitive elements like uranium and vanadium. This work highlights the profound ecosystem stresses imposed by global warming during the PETM, particularly in regions like the eastern Tethys, where intensified weathering and productivity may have exacerbated marine anoxia.

4. Biotic responses to hyperthermal events

Triassic–Paleogene hyperthermals were characterized by rapid global warming, ocean deoxygenation and acidification that caused major biological turnovers and, in many cases, mass extinctions (Song et al., 2021; Clapham and Renne, 2019; Shen et al., 2024). Today, habitats are being rapidly reshaped by current global changes, inflicting substantial damage on marine and terrestrial biodiversity (Díaz et al., 2019; Penn and Deutsch, 2022). Modern biotic extinction drivers under rapid global warming are broadly shared with those in the past hyperthermal events, and therefore, understanding how ecosystems evolve in response to climate change—past, present, and future—is an urgent challenge and disciplinary mission for Earth scientists.

The fossil record of hyperthermal events, especially from the marine environment, provide important opportunities to test for generalities in the biotic response to climatic and environmental stressors (e.g., Song et al., 2020, 2021; Foster et al., 2023). Jihede Haj Messaoud et al. (2023, this VSI; Fig. 1.2 l) investigated the response of benthic biota, particularly nummulites, to the Middle Eocene Climatic Optimum (MECO) in the southern Mediterranean. The study integrates stable isotope analysis, abundance of benthic fauna, and astrochronology to explore the relationship between climate warming and biotic changes. The results indicate that nummulites abundance peaked during the MECO warming phase, linked to eccentricity-modulated precession cycles. This warming event led to higher sea levels and a shift to arid/semi-arid climates, promoting carbonate-platform development. In contrast, marl-rich intervals reflect more humid climate conditions with lower sea levels. The study confirms that short eccentricity cycles played a dominant role in mediating regional climate during the MECO.

Das et al. (2024a, this VSI; Fig. 1.2 m) studied the ichnological response to the Middle Eocene Climatic Optimum (MECO) in the Bartonian deposits of the Kutch Basin, India. The study focuses on the ichnological and sedimentological impacts of this global warming event on the endobenthic community in a shallow-marine carbonate platform. The results reveal a significant disruption in bioturbation and bioerosion patterns, particularly through the presence of firmground and hardground horizons, along with glauconitic shales and carbonate-rich beds. The appearance of distinct trace fossils, including *Balanoglossites* and *Gastrochaenolites*, coincides with sediment starvation and hardground formation during the MECO, suggesting environmental stress due to fluctuating sea levels and basin restriction. The study provides valuable insights into the interaction between climatic events and ichnological records in marine sediments during the Eocene.

Rodríguez-Barreiro et al. (2024, this VSI; Fig. 1.2n) analyzed the lead-up and manifestation of the Oceanic Anoxic Event 2 (OAE 2) at DSDP Site 398 (Vigo Seamount, NW Iberian offshore). The study combines palynological and geochemical data to investigate shifts in terrestrial and marine ecosystems across the Cenomanian–Turonian boundary. The results highlight significant changes in the palynological assemblages, including a reduction in marine dinoflagellate cyst diversity coinciding with a positive $\delta^{13}C$ excursion. By contrast, terrestrial assemblages saw an increase in Normapolles pollen, indicating a major floral turnover. The authors suggest that these biological shifts were driven by climate changes that impacted both marine and terrestrial communities during the OAE 2.

Baranyi et al. (2024, this VSI; Fig. 1.2o) investigated the impact of the T-OAE on vegetation in the Ordos Basin, North China. This study employs high-resolution palynological data to assess plant community changes during this hyperthermal event. The results indicate that significant biodiversity loss occurred, with gymnosperm-dominated forests transitioning to more drought-resistant flora, particularly Cheirolepidiaceae. The NCIE onset during the T-OAE marks the most drastic vegetation turnover, with increased soil erosion and deforestation exacerbating terrestrial ecosystem stress. Pioneer plants, such as ferns and lycopsids, began recolonizing the disturbed habitats before the event concluded. This research highlights regional differences in vegetation responses, with the Ordos Basin experiencing aridification and climatic oscillations during the T-OAE, contributing to the collapse of terrestrial ecosystems.

5. Long-term climatic and environmental changes in greenhouse world

The longer-term background climatic and environmental conditions associated with hyperthermal are of critical importance as they likely played a key role in setting the necessary conditions for hyperthermals to occur (Landwehrs et al., 2021; Dal Corso et al., 2022; Gernon et al., 2024). Ultimately, research on the longer-term climate state spanning hyperthermal events provides a historical framework and theoretical support for understanding Earth's climate system over different geological timescales, and hence aiding in the prediction of future climate trends.

Cao et al. (2023, this VSI; Fig. 1.2p) applied aeolian architecture and sedimentary model reconstruction to investigate a Late Cretaceous intermontane desert system in South China. Their dynamic evolution modeling show that the intermontane desert transitioned from a lacustrine-dominated to an aeolian-dominated system, which indicates a gradual drying trend. They concluded that development of the intermontane desert was controlled by the Late Cretaceous greenhouse climate, the accelerated aridification of the subtropical high, and the rain shadow effect of the coastal mountains. The development of desert lake and damp/wet interdune deposits was influenced by the input of palaeo-monsoon moisture, which indicates that it might have been on

the windward side of the coastal mountains during the Late Cretaceous.

Jin et al. (2024, this VSI; Fig. 1.2q-s) applied clumped isotope (Δ_{47}) thermometry to paleosol carbonates from the central part of East China to reconstruct terrestrial paleotemperatures and atmospheric CO_2 (pCO_2) in the Middle Jurassic. The study suggests that terrestrial mean annual temperatures ranged from 30 ± 4 °C to 34 ± 4 °C and the estimated mean pCO_2 was 1219 ± 519 ppmv in mid-latitude East China during the Middle Jurassic. Comparison with global records suggests that the paleoclimate was relatively warm and stable from the Middle Jurassic to at least the earliest Cretaceous (ca. 180–135 Ma). Data collectively indicate a strong relationship between the inferred relatively stable temperatures and pCO_2 levels of the Middle Jurassic–Early Cretaceous.

Yin et al. (2023, this VSI; Fig. 1.2 k) utilized clumped isotope concentrations (Δ_{47}) and total mercury concentrations from the uppermost Cretaceous to lowermost Paleogene succession in the Nanxiong Basin (South China) to reconstruct paleotemperature and volcanic activity across the K-Pg boundary in low-latitude regions. Their findings indicate an exceptionally high mean annual terrestrial temperature of approximately 30 °C, supporting the existence of an expanded tropical zone during the K-Pg boundary. Additionally, they propose that Hg sequestration during the eruption of the Deccan Traps could have been modulated by the extremely hot and arid climate.

Xu et al. (2023, this VSI; Fig. 1.2 t) utilized microfacies analysis to demonstrate that platform geometry in South Iran transitioned from a ramp to a rimmed platform during the Cenomanian. By integrating paleobathymetry, elemental geochemistry, and carbon-isotope stratigraphy, they discovered that the evolution of platform geometry was driven by faunal changes, which were influenced by long-term eustatic changes. Additionally, they identified OAE1b, OAE1d, and Middle Cenomanian events in the region.

Das et al. (2024b, this VSI; Fig. 1.2 m) investigated the ichnological response to Early Eocene warming events (ETM 2, ETM 3, and EECO) in the Naredi Formation of the Kutch Basin, India. Their study explores ichnofossils and sedimentary sequences in a marginal-marine mixed siliciclastic-carbonate system, focusing on biotic assemblage changes due to climatic perturbations. The distinct ichnological patterns reveal a low ichnodiversity during the Early Eocene hyperthermal, especially in the lower glauconite-rich shales corresponding to oxygen-depleted environments. The upper parts of the formation exhibit a gradual increase in trace fossil diversity and abundance, correlating with improved environmental conditions during the EECO. This progression mirrors a shift from eutrophic, stressed marine settings to more oligotrophic, open marine conditions, demonstrating the gradual recovery of the benthic ecosystem. The data provide insights into how warming events impacted marine biota and sedimentation, emphasizing that ichnofossils are valuable for reconstructing paleoenvironmental changes linked to hyperthermals.

6. Concluding remarks

The 17 articles in this special issue offer broad look at the environmental and biological effects of key Mesozoic–Cenozoic rapid ancient hyperthermals (from the Permian–Triassic boundary to the Middle Eocene) and long-lasting greenhouse conditions. By integrating geochemical proxies, sedimentary records, and paleontological changes, the studies highlight increased instability in the global carbon cycle and global temperatures during past hyperthermals coupled to changing seawater redox conditions and higher primary productivity in marine, and higher chemical weathering, hydrological shifts, and more frequent wildfires on land. The studies also highlight the key role of hyperthermals in driving biotic changes both in marine and terrestrial environment. Hyperthermals are commonly linked to the emplacement of LIPs and the likely associated release of high amounts of greenhouse gases and volatiles into the atmosphere and the oceans. The findings underline how past hyperthermals can serve as analogs for understanding the potential consequences of modern climate change due to anthropogenic greenhouse gases emissions. The results emphasize the importance of applying fundamental sedimentology, geochemistry, and paleontology, as well as more modern data assimilation, mining, and Earth system modeling methods. Notably, linking environmental changes with fossil records and Earth system modeling can aid in testing causal hypotheses and assessing the pace and scale of environmental forces during hyperthermals.

CRediT authorship contribution statement

Zhong Han: Conceptualization, Data curation, Writing – original draft. **Santanu Banerjee:** Writing – review & editing. **Jacopo Dal Corso:** Writing – review & editing. **Xiumian Hu:** Funding acquisition, Project administration, Writing – review & editing. **David B. Kemp:** Writing – review & editing.

Declaration of competing interest

The authors declare that they have no known competing financial interests or personal relationships that could have appeared to influence the work reported in this paper.

Acknowledgements

This special issue was supported by the NSFC Basic Science Center Program “Continental Evolution and Earth’s Monsoon System” (grants 42488201 and 41888101). We extend our sincere thanks to *Palaeogeography Palaeoclimatology Palaeoecology* for publishing this special issue and to managing editors Howard Falcon-Lang, Alexander J. Dickson and Bing Shen for their invaluable guidance and support throughout the editorial process. We express our gratitude to the reviewers for generously dedicating their time to offer critical and insightful comments. This special issue is a contribution to the UNESCO-IUGS IGCP 739: *The Mesozoic–Palaeogene hyperthermal events*.

Data availability

No data was used for the research described in the article.

References

Baranyi, V., Jin, X., Dal Corso, J., Li, B., Kemp, D.B., 2024. Vegetation response to climate change during an early Jurassic hyperthermal event (Jenkyns Event) from Northern China (Ordos Basin). Palaeogeogr. Palaeoclimatol. Palaeoecol. 643, 112180.

Cao, S., Ma, J., Wang, C., 2023. The sedimentological characteristics of the intermontane desert system in the Jurong Basin, South China and its relationship with the late cretaceous hot climate. Palaeogeogr. Palaeoclimatol. Palaeoecol. 623, 111618.

Clapham, M.E., Renne, P.R., 2019. Flood Basalts and Mass Extinctions. Annu. Rev. Earth. Pl. Sc. 47, 275–303.

Dal Corso, J., Mills, B.J.W., Chu, D., Newton, R.J., Song, H., 2022. Background Earth system state amplified Carnian (late Triassic) environmental changes. Earth Planet. Sci. Lett. 578, 117321.

Das, M., Dasgupta, S., Srivastava, A., Rajkhowa, D., Banerjee, S., 2024a. Ichnological response to the Middle Eocene Climatic Optimum (MECO) in the Bartonian deposits of Kutch Basin, India. Palaeogeogr. Palaeoclimatol. Palaeoecol. 643, 112183.

Das, M., Dasgupta, S., Roy Choudhury, T., D’Souza, R., Banerjee, S., 2024b. Impact of early Eocene (Ypresian) warming events on ichnological assemblage of the Naredi Formation, western Kutch (Kachchh) Basin of Gujarat, India. Palaeogeogr. Palaeoclimatol. Palaeoecol. 639, 112063.

Dong, Y., Gachetti, A., Wu, Q., De Palma, M., Hu, X., Brachfeld, S., Yang, Z., Wang, J., Wang, Y., Jiang, S., Cui, Y., 2024. Paleoenvironment reconstruction of the eastern Tethys during the pre-onset excursion preceding the PETM. Palaeogeogr. Palaeoclimatol. Palaeoecol. 647, 112234.

Ernst, R.E., Youbi, N., 2017. How large Igneous Provinces affect global climate, sometimes cause mass extinctions, and represent natural markers in the geological record. Palaeogeogr. Palaeoclimatol. Palaeoecol. 478, 30–52.

Foster, G.L., Hull, P., Lunt, D.J., Zachos, J.C., 2018. Placing our current ‘hyperthermal’ in the context of rapid climate change in our geological past. Philos. T. R. Soc. A 376, 20170086.

Foster, W.J., Allen, B.J., Kitzmann, N.H., Münchmeyer, J., Rettelbach, T., Witts, J.D., Whittle, R.J., Larina, E., Clapham, M.E., Dunhill, A.M., 2023. How predictable are mass extinction events? R. Soc. Open Sci. 10, 221507.
Gernon, T.M., Mills, B.J.W., Hincks, T.K., Merdith, A.S., Alcott, L.J., Rohling, E.J., Palmer, M.R., 2024. Solid Earth forcing of Mesozoic oceanic anoxic events. Nat. Geosci. 17, 926–935.
Gradstein, F.M., Ogg, J.G., Schmitz, M.D., Ogg, G.M., 2020. Geologic Time Scale 2020. Elsevier.
He, T., Kemp, D.B., Li, J., Ruhl, M., 2023. Paleoenvironmental changes across the Mesozoic–Paleogene hyperthermal events. Glob. Planet. Chang. 222, 104058.
He, J., Hu, X., Li, J., Kemp, D.B., Hou, M., Han, Z., 2024. Millennial-scale sedimentary evolution of carbonate platforms during the Permian–Triassic boundary hyperthermal event. Palaeogeogr. Palaeoclimatol. Palaeoecol. 654, 112455.
Hu, X., Li, J., Han, Z., Li, Y., 2020. Two types of hyperthermal events in the Mesozoic–Cenozoic: Environmental impacts, biotic effects, and driving mechanisms. Sci. China Earth Sci. 63, 1041–1058.
Jenkyns, H.C., 2010. Geochemistry of oceanic anoxic events. Geochem. Geophys. Geosyst. 11, Q03004.
Jiao, S.-L., Zhang, H., Cai, Y.-F., Jin, C.-F., Shen, S.-Z., 2024. Polycyclic aromatic hydrocarbons (PAHs) evidence for frequent combustion events on land during the Permian–Triassic transition in Northwest China. Palaeogeogr. Palaeoclimatol. Palaeoecol. 642, 112152.
Jin, T., Huntington, K.W., Wen, Y., Gu, X., Schauer, A.J., Zhang, L., 2024. Clumped isotope records of terrestrial temperatures during the Middle Jurassic (180–150 Ma) in East China. Palaeogeogr. Palaeoclimatol. Palaeoecol. 637, 112014.
Judd, E.J., Tierney, J.E., Lunt, D.J., Montañez, I.P., Huber, B.T., Wing, S.L., Valdes, P.J., 2024. A 485-million-year history of Earth's surface temperature. Science 385, eadk3705.
Kovács, E.B., Ruhl, M., Silva, R.L., McElwain, J.C., Reolid, M., Korte, C., Ruebsam, W., Hesselbo, S.P., 2024. Mercury sequestration pathways under varying depositional conditions during early Jurassic (Pliensbachian and Toarcian) Karoo-Ferrar volcanism. Palaeogeogr. Palaeoclimatol. Palaeoecol. 637, 111977.
Landwehrs, J., Feulner, G., Petri, S., Sames, B., Wagreich, M., 2021. Investigating Mesozoic climate Trends and Sensitivities with a large Ensemble of Climate Model Simulations. Paleoceanogr. Paleoclimatol. 36 e2020PA004134.
Mancini, A.M., Lozar, F., Gennari, R., Capozzi, R., Morigi, C., Negri, A., 2024. The past to unravel the future: Deoxygenation events in the geological archive and the anthropocene oxygen crisis. Earth Sci. Rev. 249, 104664.
Messaoud, J.H., Thibault, N., De Vleeschouwer, D., Monkenbusch, J., 2023. Benthic biota (nummulites) response to a hyperthermal event: Eccentricity-modulated precession control on climate during the middle Eocene warming in the Southern Mediterranean. Palaeogeogr. Palaeoclimatol. Palaeoecol. 626, 111712.
Percival, L.M.E., Jenkyns, H.C., Mather, T.A., Dickson, A.J., Batenburg, S.J., Ruhl, M., Hesselbo, S.P., Barclay, R., Jarvis, I., Robinson, S.A., Woelders, L., 2018. Does large igneous province volcanism always perturb the mercury cycle? Comparing the records of Oceanic Anoxic event 2 and the end-cretaceous to other Mesozoic events. Am. J. Sci. 318, 799.
Rodríguez-Barreiro, I., Santos, A.A., Villanueva-Amadoz, U., Louwye, S., Robinson, S.A., Diez, J.B., 2024. Lead-up and manifestation of the Oceanic Anoxic Event 2 at the DSDP Site 398 (Vigo Seamount, NW Iberian offshore): Palynological and geochemical insights. Palaeogeogr. Palaeoclimatol. Palaeoecol. 647, 112223.
Scotese, C., 2021. An atlas of Phanerozoic paleogeographic maps: the seas come in and the seas go out. Annu. Rev. Earth Planet. Sci. 49 (1), 679–728. https://doi.org/10.1146/annurev-earth-081320-064052.
Shen, S., Zhang, S., Wang, W., Wang, X., Fan, J., Chen, J., Wang, B., Cao, J., Yang, S., Zhang, H., Li, G., Deng, T., Li, X., Chen, J., 2024. Deep-time major biological and climatic events versus global changes: Progresses and challenges (in Chinese). Chin. Sci. Bull. 2024 (69), 268–285.
Song, H., Huang, S., Jia, E., Dai, X., Wignall, P.B., Dunhill, A.M., 2020. Flat latitudinal diversity gradient caused by the Permian–Triassic mass extinction. Proc. Natl. Acad. Sci. 117, 17578.
Song, H., Kemp, D.B., Tian, L., Chu, D., Song, H., Dai, X., 2021. Thresholds of temperature change for mass extinctions. Nat. Commun. 12, 4694.
Tierney, J.E., Poulsen, C.J., Montañez, I.P., Bhattacharya, T., Feng, R., Ford, H.L., Hönisch, B., Inglis, G.N., Petersen, S.V., Sagoo, N., Tabor, C.R., Thirumalai, K., Zhu, J., Burls, N.J., Foster, G.L., Goddéris, Y., Huber, B.T., Ivany, L.C., Kirtland Turner, S., Lunt, D.J., McElwain, J.C., Mills, B.J.W., Otto-Bliesner, B.L., Ridgwell, A., Zhang, Y.G., 2020. Past climates inform our future. Science 370, eaay3701.
Wang, J., Li, X., Wang, Y., Zhou, Y., Zheng, C., 2024a. Long-term variations in terrestrial carbon cycles and atmospheric CO2 levels: Exploring impacts on global ecosystem and climate in the aftermath of end-cretaceous mass extinction. Palaeogeogr. Palaeoclimatol. Palaeoecol. 643, 112177.
Wang, Y., Jiang, S., Cui, Y., Liang, R., Su, H., 2024b. Elevated Sea surface temperature and enhanced primary productivity during Ocean Anoxic Event 1d in the eastern Tethys: Calcareous nannofossil evidence from southern Tibet, China. Palaeogeogr. Palaeoclimatol. Palaeoecol. 654, 112418.
Westerhold, T., Marwan, N., Drury, A.J., Liebrand, D., Agnini, C., Anagnostou, E., Barnet, J.S.K., Bohaty, S.M., De Vleeschouwer, D., Florindo, F., Frederichs, T., Hodell, D.A., Holbourn, A.E., Kroon, D., Lauretano, V., Littler, K., Lourens, L.J., Lyle, M., Pälike, H., Röhl, U., Tian, J., Wilkens, R.H., Wilson, P.A., Zachos, J.C., 2020. An astronomically dated record of Earth's climate and its predictability over the last 66 million years. Science 369, 1383–1387.
Wu, Q., Cui, Y., Wang, Y., Jiang, S., Dong, Y., Shen, J., 2024. Biogeochemical responses to global warming during the Paleocene–Eocene Thermal Maximum in the eastern Tethys. Palaeogeogr. Palaeoclimatol. Palaeoecol. 636, 111969.
Xu, Y., Hu, X., Garzanti, E., Sun, G., Jiang, J., Li, J., Zhang, S., Schlagintweit, F., Rao, X., 2023. Carbonate factories and their critical control on the geometry of carbonate platforms (mid-cretaceous, southern Iran). Palaeogeogr. Palaeoclimatol. Palaeoecol. 625, 111680.
Yang, Y., Han, Z., Hu, X., He, T., Newton, R.J., Harvey, J., 2024. Strontium isotope evidence for regional enhanced continental weathering during the early Toarcian in the Tethys Himalaya. Palaeogeogr. Palaeoclimatol. Palaeoecol. 641, 112136.
Yin, Y., Zhang, L., Gu, X., Yin, R., Wen, Y., Jin, T., Wang, C., 2023. High terrestrial temperature in the low-latitude Nanxiong Basin during the Cretaceous-Paleogene boundary interval. Palaeogeogr. Palaeoclimatol. Palaeoecol. 617, 111489.